Low dose dietary contamination with deoxynivalenol mycotoxin exacerbates enteritis and colorectal cancer in mice.

Madjid Djouina, Christophe Waxin, Segolene Caboche, Karine Lecointe, A. Steimle, Delphine Beury, M. S. Desai, David Hot, Laurent Dubuquoy, David Launay, et al.

Science of the Total Environment 900 (2023) 165722

Contents lists available at ScienceDirect

Science of the Total Environment

journal homepage: www.elsevier.com/locate/scitotenv

Low dose dietary contamination with deoxynivalenol mycotoxin exacerbates enteritis and colorectal cancer in mice

Madjid Djouina [a], Christophe Waxin [a], Ségolène Caboche [b], Karine Lecointe [c], Alexander Steimle [d], Delphine Beury [b], Mahesh S. Desai [d], David Hot [b], Laurent Dubuquoy [a], David Launay [a], Cécile Vignal [a], Mathilde Body-Malapel [a,*]

[a] Univ. Lille, Inserm, CHU Lille, U1286- INFINITE - Institute for Translational Research in Inflammation, F-59000 Lille, France
[b] Univ. Lille, CNRS, Inserm, CHU Lille, Institut Pasteur de Lille, US41-UAR 2014-PLBS, F-59000 Lille, France
[c] Inserm U1285, Univ. Lille, CHU de Lille, UMR CNRS 8576 - UGSF - Unité de Glycobiologie Structurale et Fonctionnelle, 59000 Lille, France
[d] Department of Infection and Immunity, Luxembourg Institute of Health, Esch-sur-Alzette, Luxembourg

ARTICLE INFO

Editor: Lidia Minguez Alarcon

Keywords:
Deoxynivalenol
Mycotoxin
Enteritis
Colorectal cancer
Tumorigenesis
Microbiota

ABSTRACT

Background: The mycotoxin deoxynivalenol (DON) is a frequent contaminant of grain and cereal products worldwide. Exposure to DON can cause gastrointestinal inflammation, disturb gut barrier function, and induce gut dysbiosis *in vivo* under basal conditions, but little is known about the effects of DON ingestion in individuals with pre-existing gastrointestinal disease.

Objectives: Mice were orally exposed to 10 and 100 μg/kg bw/day of DON, corresponding to 10 to 100-fold human tolerable daily intake concentrations, and to the translation in mice of current human daily intake. The effects of DON exposure were explored under steady-state conditions, and in murine models of enteritis and colorectal cancer (CRC).

Results: After 8 days of DON exposure, an increase of histomorphological and molecular parameters of epithelial proliferation were observed in normal mice, from the duodenum to the colon. The same exposure in a murine model of indomethacin-induced enteritis led to exacerbation of lesion development and induction of ileal cytokines. DON exposure also worsened the development of colitis-associated CRC in mice as shown by increases in endoscopic and histological colitis scores, tumor grades, and histological hyperplasia. In colon of DON-exposed mice, upstream and downstream ERK signaling genes were upregulated including Mapk1, Mapk3, Map 2k1, Map2k2 core ERK pathway effectors, and Bcl2 and Bcl2l1 antiapoptotic genes. The effects observed in the CRC model were associated with alterations in cecal microbiota taxonomic composition and metabolism of bacterial fucose and rhamnose. Strong Spearman's correlations were revealed between the relative abundance of the changed bacterial genera and CRC-related variables.

Discussion: Ingestion of DON mycotoxin at concentrations representative of human real-world exposure worsened the development of indomethacin-induced enteritis and colitis-associated CRC in mice. Our results suggest that even at low doses, which are currently tolerated in the human diet, DON could promote the development of intestinal inflammatory diseases and CRC.

1. Introduction

Mycotoxins are naturally occurring secondary metabolites produced by fungi. They cause a variety of adverse health effects for both humans and livestock, ranging from acute poisoning to long-term effects such as immune or reproductive deficiencies and cancer (De Ruyck et al., 2015; Liao et al., 2018; Yang et al., 2019). Deoxynivalenol (DON) is one of the most ubiquitous mycotoxins worldwide (Chen et al., 2019). DON is a type-B trichothecene mycotoxin, mainly produced by *Fusarium graminearum, Fusarium culmorum,* and *Fusarium crookwellense* (Woelflingseder et al., 2019). Fusarium species infect cereal grains such as wheat, maize, barley, and oats. Since DON is only partially destroyed by high

* Corresponding author at: Institute for Translational Research in Inflammation, INFINITE - Univ. Lille, Inserm, CHU Lille U1286, Faculté de Médecine - Pôle Recherche, 4éme étage Centre, Place Verdun, F-59045 Lille Cedex, France.
E-mail address: mathilde.body@univ-lille.fr (M. Body-Malapel).

https://doi.org/10.1016/j.scitotenv.2023.165722
Received 1 June 2023; Received in revised form 20 July 2023; Accepted 20 July 2023
Available online 22 July 2023

temperature during processing, it is detected in feeds (Kamle et al., 2022; Zhao et al., 2021) but also in human processed food and beverage products such as breakfast cereals, bread, pizza, beer, and wine (Wang et al., 2019).

The gastrointestinal toxicity of DON is attributed to different mechanisms. The toxicity of DON is partly related to its ability to disrupt eukaryotic protein synthesis *via* binding to the peptidyl transferase site of the ribosome, a process known as the ribotoxic stress response (RSR) (Hooft and Bureau, 2021). DON binding to ribosomes inhibit protein translation and activates mitogen-activated protein kinases (MAPKs) (Pinton et al., 2010; Wang et al., 2018; Zhang et al., 2020). The MAPK family comprises several subfamilies of signaling proteins including MAPK3,1 (ERK1,2), MAPK 8,9,10 (JNK 1,2,3), MAPK14,11,12,13 (p38α/β/γ/δ) (Lavoie et al., 2020), and they are crucial to the pro-inflammatory gene expression and apoptosis induced by DON (Lee et al., 2019; Wang et al., 2023; Zhang et al., 2020). Activation of ERK plays a pivotal role in inducing cell motility, proliferation, differentiation, and survival, whereas p38 is closely related to cell cycle progression and cell differentiation (Lavoie et al., 2020; Phan et al., 2023). The excessive oxidative stress (You et al., 2021), mitochondrial dysfunction (Wang et al., 2021), and ferroptosis induction (Liu et al., 2023) are pivotal factors of DON gastrointestinal toxicity. The adverse effects induced in mammals by dietary DON contamination on the intestinal tract has been the focus of increasing awareness and investigation. Notably, in mice, low DON concentration (25 μg/kg bw/day for 30 days) was shown to trigger systemic and duodenal upregulation of Il-1β secretion (Tardivel et al., 2015), and a lower dose (10 μg/kg bw/day for 9 months) induced histomorphological and immune impairments of the intestinal tract and provoked dysbiosis (Vignal et al., 2018). More recently, dietary DON exposure (8 mg/kg food for 4 weeks) was shown to exacerbate the development of dextran sodium sulfate (DSS)-induced colitis in rats which was associated with an increased pro-inflammatory response in spleen and colon (Payros et al., 2020).

Exposure to DON can disturb gut barrier function and induce gut dysbiosis and inflammation in healthy individuals, but less is known about the effects of DON on those with pre-existing gastrointestinal disease. To better understand the etiology of DON-related health effects, we profiled molecular and physiological endpoints in murine models of induced enteritis and colorectal cancer.

2. Material and methods

2.1. Mice and experimental design

Male C57BL/6 mice (aged 7 weeks) were purchased from Janvier Labs (Le Genest-Saint-Isle, France) and housed under standard conditions. Mice were randomly assigned to experimental groups. Mice received 0, 10, or 100 μg/kg bw/day of DON (Cayman Chemical, Ann Arbor, MI, USA) diluted in their drinking water for 8-day treatments or in food for 90-day treatments (referred to as the control, 10 μg DON, and 100 μg DON groups, respectively).

2.2. Induction and macroscopic evaluation of small intestinal inflammation induced by indomethacin

To induce small intestinal injury, 20 mg/kg bw indomethacin (Sigma-Aldrich, St. Louis, MO, USA) dissolved in 0.5 % carboxymethyl cellulose was orally administered to mice (Body-Malapel et al., 2019; Xiao et al., 2017). 24 h after indomethacin injection, mice were intravenously administered with 1 % Evans Blue dye (Sigma-Aldrich) in 0.9 % NaCl to visualize macroscopic lesions, and animals were sacrificed 30 min later. At necropsy, ileum, jejunum, and duodenum were separately harvested, longitudinally incised, photographed, and then immediately frozen for future analysis. The number and area of lesions were quantified using Image J software (NIH, USA).

2.3. Induction and macroscopic evaluation of azoxymethane (AOM)-DSS induced colorectal cancer

Mice were injected i.p. with 10 mg/kg AOM. After 5 days, 1.5 to 3 % DSS (TdB Labs, Ultuna, Sweden) was added to drinking water for a period of 5 days, followed by regular drinking water for 2 weeks. This cycle was repeated 3 times and mice were sacrificed 40 days after the last DSS cycle. At necropsy, colon tissue was harvested, longitudinally incised, and photographed. Macroscopically visible tumors were counted and measured using Image J software.

2.4. Histological analyses of intestinal and colon tissues

Colon, ileum, jejunum, and duodenum samples were fixed in 10 % buffered formalin for 24 h, processed, and embedded in paraffin wax by an automatic sample preparation system (LOGOS One, Milestone Medical, Sorisole, Italy). Serial histological sections of 4 μm thickness were cut, deparaffinized, rehydrated, and stained with May Grünwald-Giemsa (MGG) for morphometric analysis under a light microscope (DM5500B; Leica Microsystems, Nanterre, France).

For steady-state experiments, measurements of duodenal, jejunal, and ileal villus height, crypt depth, and colonic mucosal surface area were performed using ImageJ software. At least 50 well-oriented mucosa, villi, and crypts were measured in at least 5 individual mice from each group of the study.

For AOM-DSS-induced colorectal cancer, colitis scores of each segment were assigned based on the extent and severity of inflammation, ulceration, and hyperplasia of the mucosa as previously described (Zaki et al., 2010). Hyperplasia scores were assigned as follows: 0 = normal (within normal limits); 1 = mild (crypts two to three times normal thickness, normal epithelium); 2 = moderate (crypts two to three times normal thickness, hyperchromatic epithelium, reduced goblet cells, scattered arborization); 3 = severe (crypts more than four times normal thickness, marked hyperchromasia, few to no goblet cells, high mitotic index, frequent arborization).

2.5. Assessment of colitis and tumorigenesis using colonoscopy

Colitis progression and tumor development were assessed using a high-resolution colonoscope (1.9 mm outer diameter; Karl Storz, Tuttlingen, Germany) at days 40, 51, 70, and 90. Mice were anesthetized using isoflurane for the duration of the procedure and closely monitored. Colitis severity was measured from recorded videos in a blinded fashion using 5 parameters described by Becker et al. (2005), including thickening of the colon, vasculature pattern, presence of fibrin, granularity of mucosal surface, and stool consistency. Each parameter was scored in a blinded fashion from 0 to 3 (with increasing severity) and totaled. Tumors observed from colonoscopy videos were counted, measured, and categorized into size: low-grade (grade 1 = very small but detectable tumor); medium-grade (grade 2 = tumor covering up to one-eighth of the colonic circumference; and grade 3 = tumor covering up to a quarter of the colonic circumference); and high-grade (grade 4 = tumor covering up to half of the colonic circumference; and grade 5 = tumor covering more than half of the colonic circumference).

2.6. Proliferating cell nuclear antigen (PCNA) immunohistochemistry

For antigen unmasking of formalin-fixed samples, sections were placed in 10 mM sodium citrate buffer (pH 6.0) and incubated in a heat-induced antigen retrieval chamber for 20 min at 121 °C. After washing, sections were blocked for 30 min with 5 % bovine serum albumin in PBS, stained overnight at 4 °C with anti-PCNA antibody (1:50 dilution of NB600-1331; Novus Biologicals, Centennial, CO, USA), and incubated with Alexa Fluor 488 or 594 conjugated secondary antibody (1:200 dilution; Invitrogen, Waltham, MA, USA) for 1 h. Sections were counterstained with DAPI (Molecular Probes, Eugene OR, USA). To ensure

specificity of immunostaining, control sections underwent simultaneous staining without primary antibody. Quantification of positive PCNA-stained cells was performed randomly using Image J software. Images were acquired with a DM5500B microscope equipped with a DFC 310 FX camera (Leica Microsystems) and mucosal layers were photographed at a magnification of 40×.

2.7. Gene expression in tissues

Total mRNA from intestinal and colon samples was extracted using a Nucleospin RNA kit (Macherey-Nagel, Dueren, Germany). Reverse transcription was performed using a High Capacity cDNA Archive Kit and quantitative polymerase chain reaction with SYBR Green (Life Technologies, Carlsbad, CA, USA). The primer sequences were designed using Primer Express 3 (Life Technologies) and are available upon request. Melting curve analyses were performed for each sample and gene to confirm the specificity of amplification. Because exposure to DON did not cause any significant alterations in *Polr2a* mRNA expression, the relative expression of each gene of interest was normalized relative to the expression of this gene. The quantification of the target gene expression was based on the comparative cycle threshold (Ct) value. The fold changes in the target genes were analyzed by the $2^{-\Delta\Delta Ct}$ method (Livak and Schmittgen, 2001).

2.8. Bacterial DNA extraction and sequencing

Genomic DNA was extracted from the cecal luminal content using a DNA stool kit (Macherey-Nagel). The quantity and purity of DNA (expressed as the ratio of absorbance at 260 nm and 280 nm (A260/A280)) were assessed using a Nanodrop® spectrophotometer (Thermo Fisher Scientific, Waltham, MA, USA). The sequencing library was generated by amplifying the V3-V4 region of the bacterial 16S-rRNA gene using 16S rRNA amplicon generation for MiSeq with the primers Bact-0341 (CCTACGGGNGGCWGCAG) and Bact-0785 (GACTACHVGGGTATCTAATCC). Individual samples were barcoded, pooled to construct the sequencing library, and sequenced using a MiSeq instrument (Illumina, San Diego, CA, USA) to generate paired-end 2 × 300 bp reads.

2.9. Analysis of sequencing data

Bioinformatic analyses were performed using the QIIME2 pipeline (version 2020.2) (Bolyen et al., 2019). The Divisive Amplicon Denoising Algorithm (DADA-2) plug-in in QIIME2 was used to filter, dereplicate, identify chimeric sequences, and merge paired-end reads to obtain a set of amplicon sequence variants (ASVs) for each sample (Callahan et al., 2016). Then representative sequences were selected for each ASV. The classify-sklearn plug-in in QIIME2, with the Silva database (version 132), was applied to assign a taxonomic annotation to each representative ASV sequence. In the next step, ASVs identified as eukaryotic contamination (none), and external contamination identified with the decontam package (57 ASVs; 3745 reads), were filtered out (Davis et al., 2018). Diversity metrics (α and β diversity) were obtained with the QIIME2 core-metrics-phylogenetic plug-in, with p-sampling depth parameter fixed to 14,616 reads which corresponded to the total frequency that each sample should be rarefied to prior to computing diversity metrics. This sampling depth allowed retention of >70 % of reads and only two samples were discarded. Tests for differential relative abundance were performed with ANCOM and corncob at the order, family, and genus levels (Mandal et al., 2015; Martin et al., 2020).

To retrieve functional profiles for the ASV data, sequences and abundance tables were used as inputs for Phylogenetic Investigation of Communities by Reconstruction of Unobserved States 2 (PICRUSt2) software analysis (Douglas et al., 2020). The differentially abundant Metacyc pathways were identified using ALDEx2 (Fernandes et al., 2014). ALDEx2 outputs the effect size which indicates the direction and volume of change of the centered log ratios. In our study, a positive sign indicated that the feature was more abundant in the 100 μg DON group whereas a negative sign indicated greater abundance in the control group.

2.10. Measurement of luminal fucose and rhamnose content

Stool samples were solubilized in PBS with 0.05 % Tween® 20 and centrifuged for 10 min at 10,000*g*. Soluble fractions were freeze-dried and then methanolysis (MeOH with 0.5 N HCl) was performed at 80 °C for 18 h. A dot of silver carbonate (Sigma-Aldrich) was added with acetic anhydride (Sigma-Aldrich) overnight. The methanolic phase was washed with heptane. Finally, derivatization was performed using a 99:1 mixture of BSTFA-TMCS and pyridine (Sigma-Aldrich). The resulting monosaccharides were analyzed by gas chromatography/mass spectrometry (GC/MS) (Agilent Technologies, Santa Clara, CA, USA) using a SOLGEL-1MS column (30 m × 0.25 mm i.d.; SGE Analytical Science, Trajan Scientific and Medical, Morrisville, NC, USA). The temperature of the column increased from 120 °C to 240 °C at a rate of 2 °C per min and a terminal level during 10 min. Myo-inositol (Sigma-Aldrich) was used as an internal standard.

2.11. Measurement of luminal fucosidase activity

Fucosidase activity was assessed in stool samples according to a previously described protocol (Steimle et al., 2021).

2.12. Statistical analyses

Data are presented as the mean ± standard error of the mean. Comparisons between different treatment groups were performed using the nonparametric Mann-Whitney *U* test. Spearman's correlation and other statistical analyses were performed using Prism 8 software (GraphPad, San Diego, CA, USA). Sequencing data was analyzed using the Wilcoxon Rank Sum test, with Benjamini-Hochberg correction for multiple testing. Statistical significance was defined as $p < 0.05$.

3. Results

3.1. Short-term exposure to low DON concentration induces epithelial proliferation in colon and small intestine

To assess the effects of short exposure to DON on intestinal homeostasis, mice were exposed to DON for 8 days. Mucosal surface area was significantly increased in the 100 μg DON group compared to control mice (Fig. 1A and B). To confirm alterations in epithelial proliferation, PCNA expression was assessed in colon sections (Fig. 1C). A significant enhancement of PCNA staining in the 100 μg DON group compared with control mice was observed (Fig. 1D). Neither mucosal surface area nor PCNA staining were significantly different in the 10 μg DON group relative to controls.

For analysis of the small intestine, villi and crypts were measured. In duodenum, jejunum, and ileum, the size of villi did not vary in mice exposed to DON compared with control mice (Fig. 1E). However, crypt size was higher in DON-exposed mice in the three intestinal tissues (Fig. 1F). Oral exposure at both dosages consistently decreased the villi/crypt ratio in duodenum, jejunum, and ileum (Fig. 1G). A significant enhancement of PCNA staining was observed in the ileum, jejunum, and duodenum of DON-exposed mice at both dosages (Fig. 1H–I). In summary, after 8 days of DON ingestion epithelial proliferation was enhanced in colon in the 100 μg DON group and in small intestine in both treatment groups.

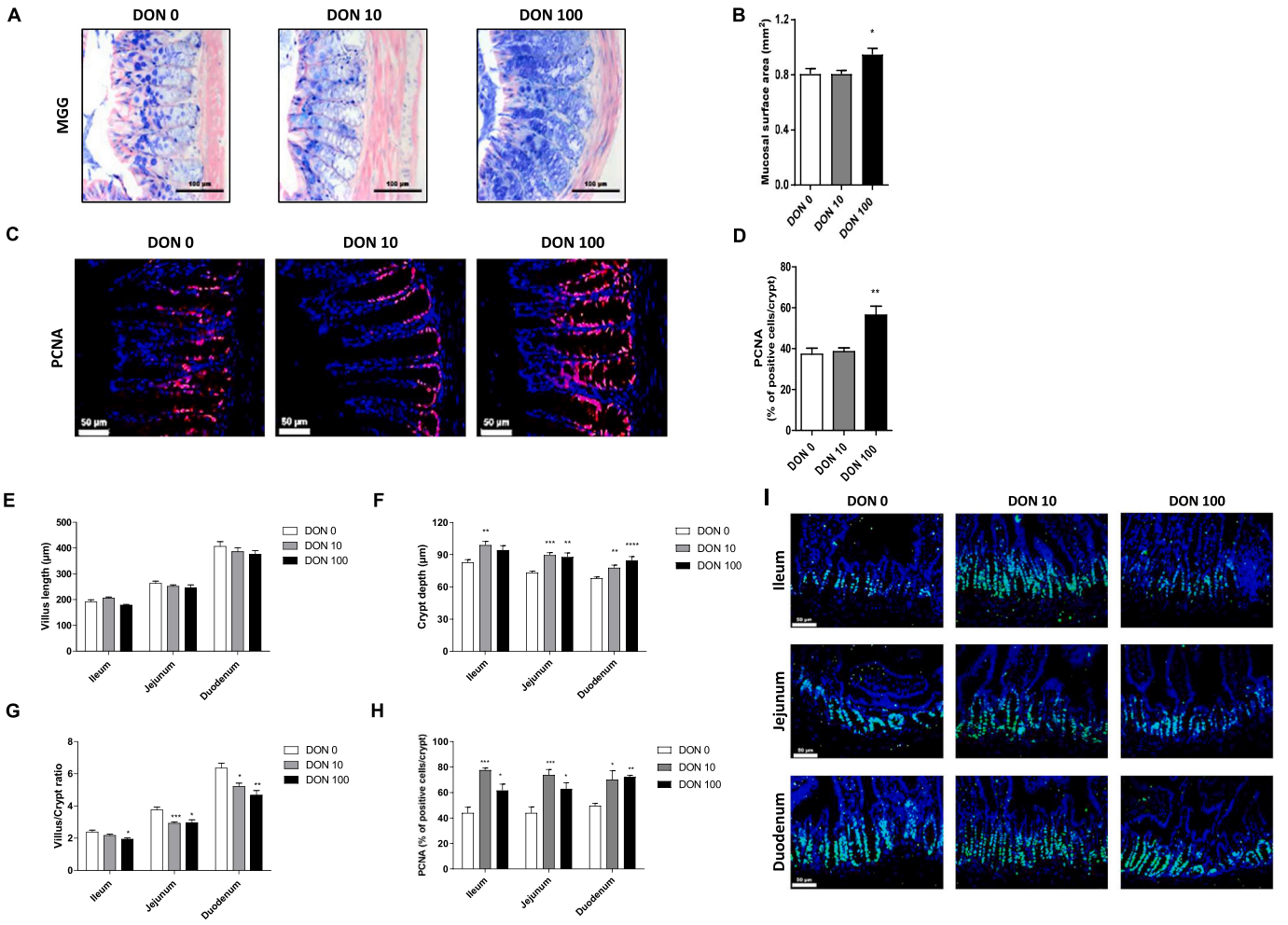

Fig. 1. Effect of 8-day deoxynivalenol (DON) exposure on colon and small intestine histomorphology and proliferating cell nuclear antigen (PCNA) expression (0, 10, and 100 µg DON/kg bw/day groups; $n = 10$ per group). (A–B) Histomorphological assessment of May Grünwald-Giemsa (MGG)-stained colon sections including (A) representative images, and (B) quantification of mucosal area. (C) PCNA immunostaining of colon sections (*red*). (D) Quantification of PCNA-positive cells. (E–G) Histomorphological assessment of May Grünwald-Giemsa-stained ileum, jejunum, and duodenum sections including (E) villus length, (F) crypt depth, and (G) villus/crypt ratio. (H–I) PCNA immunostaining of small intestine sections (*green*) including (H) quantification of PCNA positive cells, and (I) representative images. Data are from two independent experiments. *$p < 0.05$, **$p < 0.01$, ***$p < 0.005$, and ****$p < 0.001$ compared to the DON 0 group as determined by the Mann-Whitney *U* test.

3.2. Short-term exposure to low DON concentration exacerbates indomethacin-induced enteritis

To investigate whether DON exposure intensifies small intestine inflammation, the effect of 8-day DON exposure on the severity of indomethacin-induced enteropathy was examined (Fig. 2A). Enteritis was induced by oral gavage with indomethacin and monitored 24 h later. Ulcerative lesions were observed, particularly in the ileum and jejunum, and these lesions were more extended in mice exposed to DON compared to control mice (Fig. 2B–C). DON oral administration induced gene expression of inflammatory cytokines in small intestine of mice, with significant increases of Tnfα, Il1β and Ifnγ levels in ileum of mice of both DON treatment groups (Fig. 2D–F). Therefore, DON exposure enhanced enteritis in this experimental model of indomethacin-induced enteritis.

3.3. Chronic DON exposure exacerbates AOM-DSS-induced colorectal carcinogenesis

The impact of DON exposure on colitis-associated carcinogenesis was investigated. In the first set of experiments, wild-type mice were treated with AOM, 1 cycle of 1.5 % DSS then 2 cycles of 2.5 % DSS, and concomitantly exposed to DON at 10 and 100 µg/kg bw/day for 90 days (Fig. 3A). The development of colitis was monitored by colonoscopy. Mice in the 100 µg DON group had significantly increased colitis scores on days 40, 51, 70, and 90 compared to controls (Fig. 3B). At the culmination of the experiment on day 90, all parameters for colitis assessment were significantly elevated, resulting in a considerable increase in the colitis score for the 100 µg DON group compared to controls (Fig. 3C–E). The total colitis histological score was significantly greater in mice exposed to both dosages of DON compared to untreated mice.

The effect of DON exposure on colorectal cancer development was also investigated. The total number of tumors rose over time without significant variations between the experimental groups (Fig. 4A). However, after 90 days of exposure, a decrease in low-grade tumors numbers and significant increase in medium- and high-grade tumors numbers was found for mice in the 100 µg DON group compared to control mice, and a dose-dependent effect was observed (Fig. 4B–C).

The second chronic study involved a more severe induction of colorectal cancer (3 % DSS, Fig. 5A–C). The number of colon tumors at day 90 was significantly increased in DON-intoxicated mice compared to control mice (Fig. 5B). Although the number of tumors <1 mm did not vary between the control and treatment groups, there was an increase of

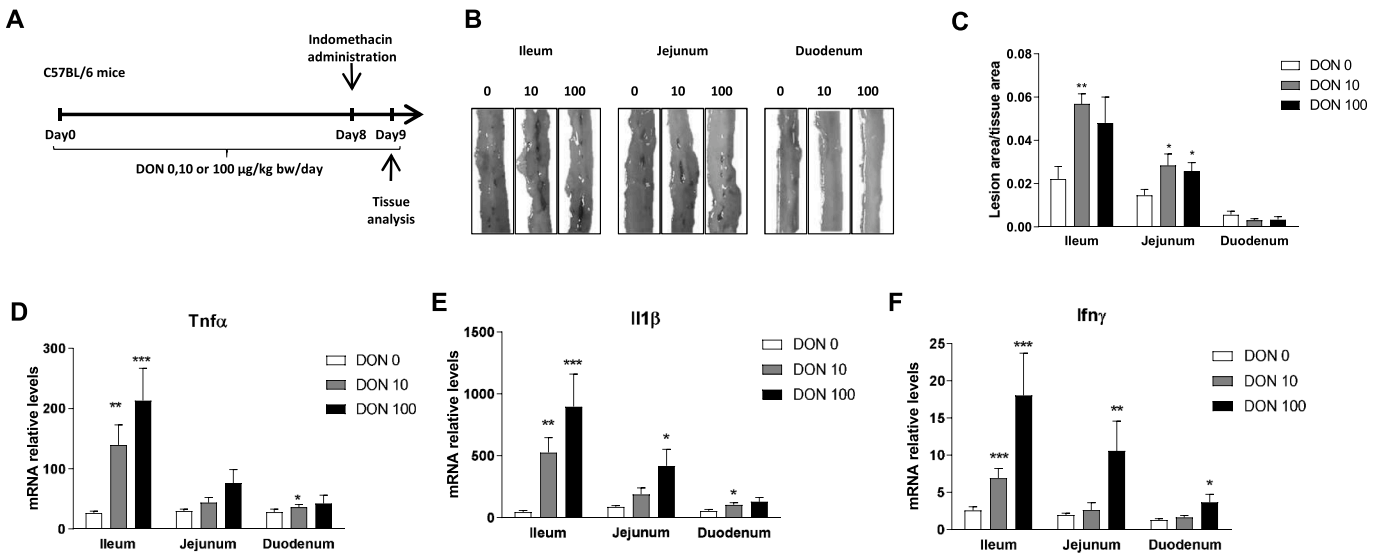

Fig. 2. Effect of 8-day deoxynivalenol (DON) exposure on indomethacin-induced enteritis (0, 10, and 100 µg DON/kg bw/day groups; n = 10 per group). (A) Experimental design. (B) Representative images of intestinal lesions. (C) Quantification of lesion area/tissue area ratio. (D–F) Quantification of intestinal mRNA levels of (D) Tnfα, (E) Il1β and (F) Ifnγ. Data are from two independent experiments. *p < 0.05, **p < 0.01, and ***p < 0.005 compared to the DON 0 group as determined by the Mann-Whitney *U* test.

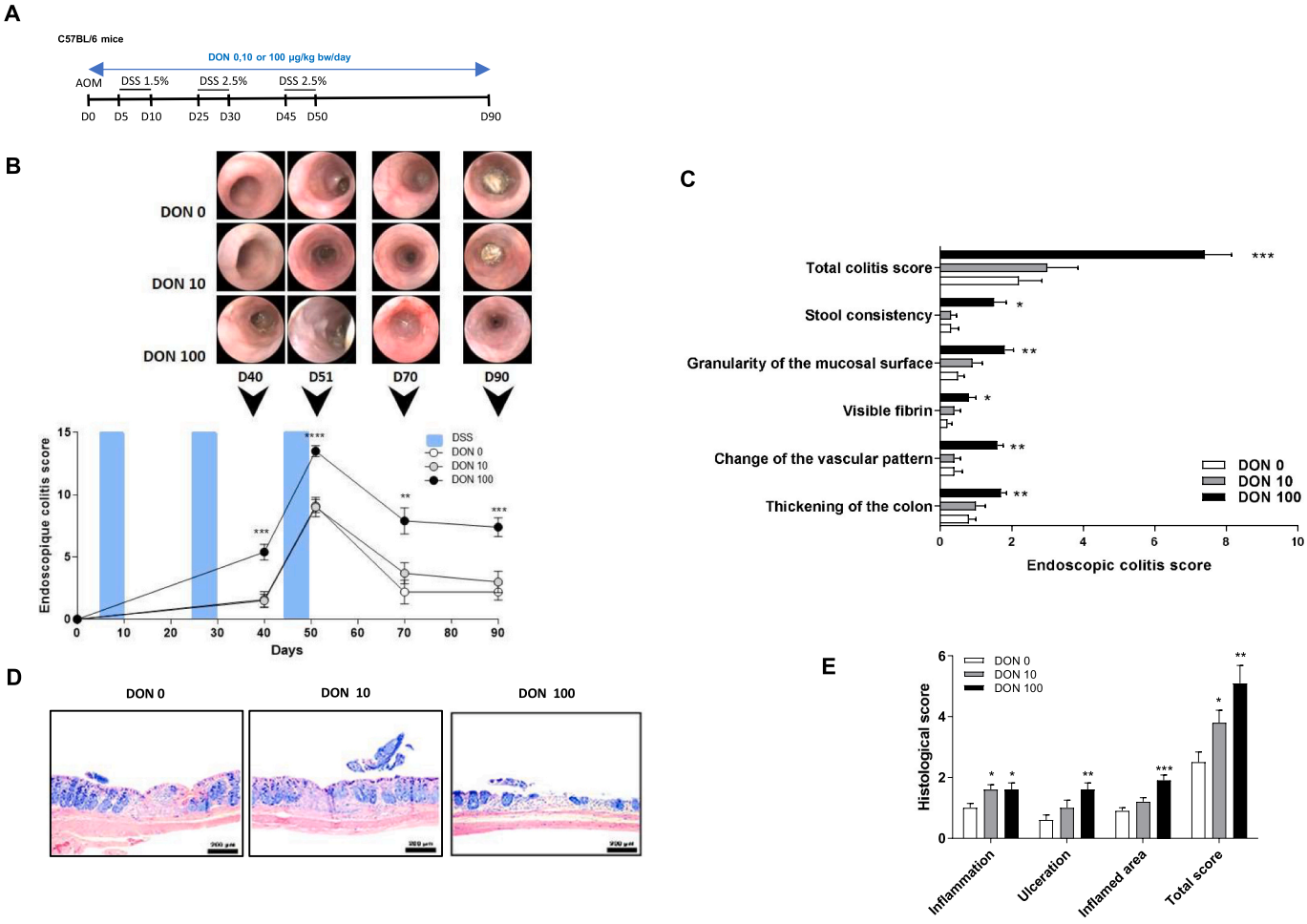

Fig. 3. Effects of chronic exposure to deoxynivalenol (DON) in the development of colitis in the azoxymethane/dextran sodium sulfate-induced model of colorectal cancer (0, 10, and 100 µg DON/kg bw/day groups; n = 10 per group). (A) Experimental design. (B) Follow-up endoscopic scoring of colitis intensity including endoscopic scores and their representative video captures. (C) Detailed endoscopic colitis scores at the experimental endpoint. (D–E) Histological assessment of colitis including (D) representative May Grünwald-Giemsa-stained colon sections, and (E) the colitis histological score. *p < 0.05, **p < 0.01, and ***p < 0.005 compared to the DON 0 group as determined by the Mann-Whitney *U* test.

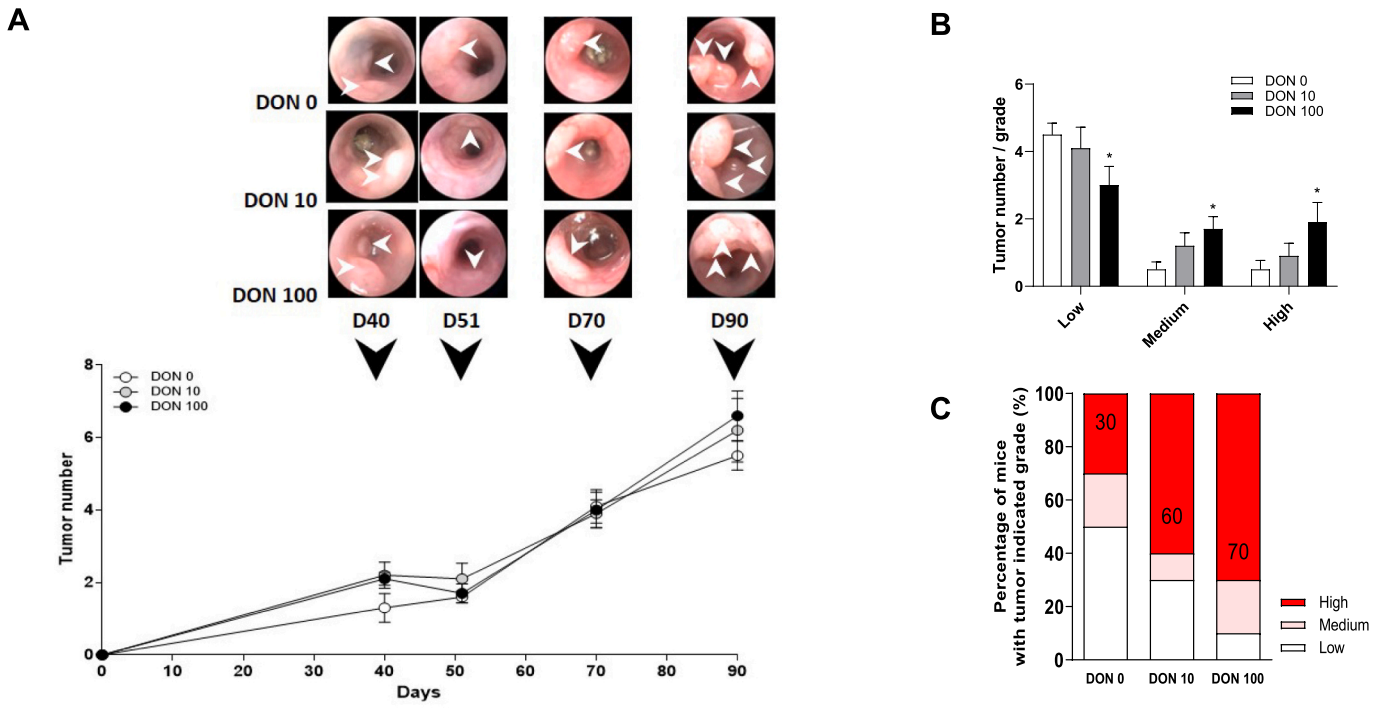

Fig. 4. Endoscopic assessment of protumorigenic effects of deoxynivalenol (DON) exposure in colorectal cancer (0, 10, and 100 μg DON/kg bw/day groups; n = 10 per group). (A) Follow-up endoscopic scoring of tumorigenesis: endoscopic score and their representative video captures. White arrows refer to tumors. (B) Number of tumors according to their grade. (C) Percentage of mice with tumor indicated grade as worse tumor grade. *p < 0.05 compared to DON 0 group as determined by the Mann-Whitney *U* test.

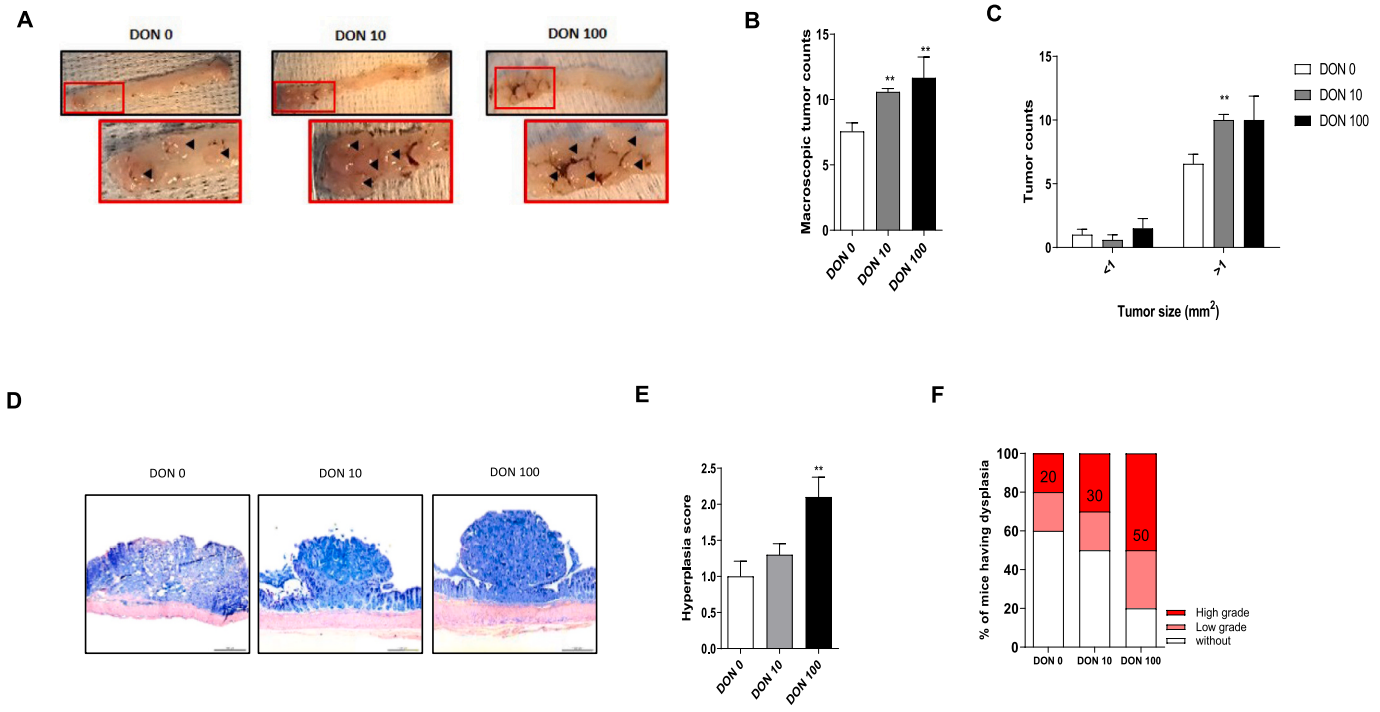

Fig. 5. Macroscopic and histological assessments of the protumorigenic effects of deoxynivalenol (DON) exposure on colorectal cancer (0, 10, and 100 μg DON/kg bw/day groups; n = 10 per group). (A–C) Macroscopic assessment of tumorigenesis including (A) representative colon images, black arrows refer to tumors. (B) macroscopic count of tumors, and (C) tumor counts by size. (D–F) Histological assessment of tumorigenesis including (D) representative May Grünwald-Giemsa-stained colon sections, (E) hyperplasia scores, and (F) percentage of mice with dysplasia. **p < 0.01 compared to the DON 0 group as determined by the Mann-Whitney *U* test.

tumors >1 mm in mice exposed to DON (Fig. 5C). At the histological level, severity of hyperplasia was significantly higher in colon of the 100 μg DON group compared to control mice (Fig. 5D–E). In a dose-dependent manner, DON exposure was associated with an increase of mice with high-grade dysplasia and a decrease of mice with low-grade or no dysplasia (Fig. 5F). These results show that ingestion of DON at 100 μg/kg bw/day worsened intensity of colitis and tumorigenesis in this murine model of AOM-DSS-induced colorectal cancer.

Activation of ERK signaling pathway has been demonstrated as mediating the effects of DON (Pinton et al., 2010; Wang et al., 2018; Zhang et al., 2020). Therefore, we assessed whether the ERK signaling genes were modulated by DON exposure in the model of AOM-DSS-induced colorectal cancer (Suppl Fig. 1). The level of genes encoding ERK2 and ERK1, Mapk1 and Mapk3 respectively, were significantly higher in both CRC groups exposed to DON compared to control CRC group. DON exposure significantly upregulated upstream genes, the dual specificity mitogen-activated protein kinase kinase 1 and 2 (Map2k1 and Map2k2), encoding MEK1 and MEK2 respectively. MAP-interacting kinase 1 and 2 (Mknk1 and Mknk2) transcripts were both enhanced in the 100 μg DON group, Mknk2 was also higher in the 10 μg DON group. Among the ERK target genes involved in cell proliferation, in accordance with an increased cell proliferation, ETS domain-containing protein Elk-1 (Elk1) and ETS domain-containing transcription factor ERF (Erf) showed respectively an upregulation and down-regulation trend, and transcriptional regulator ERG (Erg) and ETS translocation variant 1 (Etv1) were upregulated in DON-exposed CRC groups. DON exposure enhanced the relative expression of Apoptosis regulator Bcl-2 (Bcl2) and Bcl-2-like protein 1 (Bcl2l1) antiapoptotic factors. The RNA polymerase I-specific transcription initiation factor (Rrn3) and the regulatory-associated protein of mTOR (Rptor) genes, involved in ERK regulation of cell growth, were upregulated in DON-exposed CRC groups compared to control CRC group. These results suggest that ERK signaling pathway could participate to DON dysregulation of cell proliferation and survival in the AOM-DSS colorectal cancer model.

3.4. DON effects on the gut microbiome

16S rRNA gene-based analysis was used to profile bacterial microbiota in mouse cecal content (Fig. 6). For the 4 α-diversity indices tested, biodiversity was significantly higher in colorectal cancer (CRC) mice exposed to DON compared to control CRC mice (Fig. 6A). In addition to α-diversity, the unweighted Unifrac distance and Bray-Curtis dissimilarity matrix were analyzed to compare similarities among gut microbial communities (β-diversity; Fig. 6B). A significant clustering was found in the principal coordinate analysis plots of these two indices showing that DON treatment at both dosages altered bacterial community structure.

ANCOM (Fig. 6) and corncob (Suppl Figs. 2–4) algorithms were used to investigate relative differences in taxonomic abundance between the three study groups. ANCOM incorporates the compositionality of microbiome data, has a low-false-positive rate, and allows covariate adjustment. Results show the differential abundance of taxa in DON-exposed CRC mice compared to control CRC mice. The order *Anaeroplasmatales* was less abundant in the 10 μg DON group (Fig. 6C). The order *Campylobacterales* was enriched in mice in both DON treatment groups. At the family level, *Anaeroplasmataceae* was found to be less

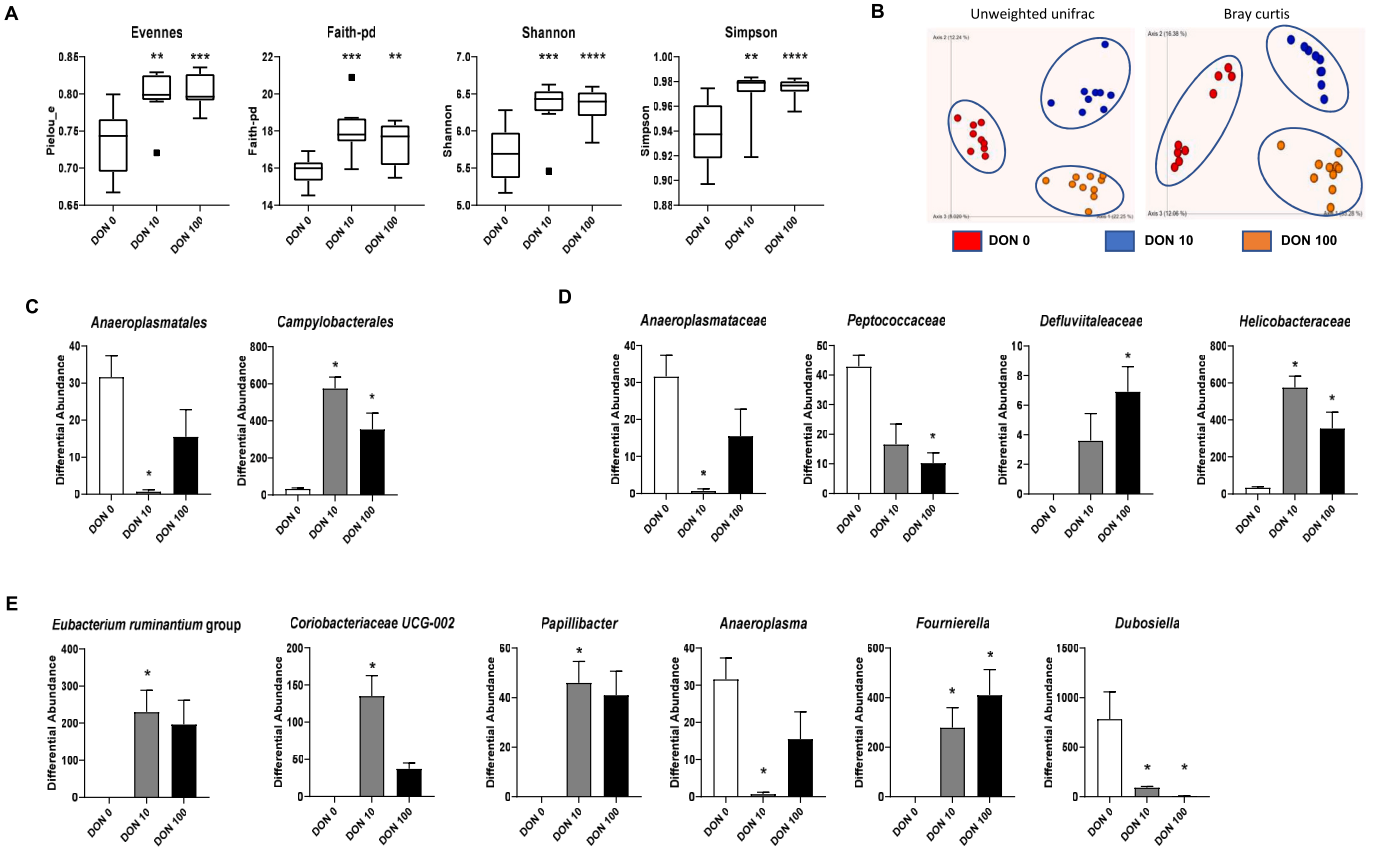

Fig. 6. Effects of deoxynivalenol (DON) exposure on cecal content microbiome of mice with colorectal cancer (0, 10, and 100 μg DON/kg bw/day groups; n = 10 per group). (A) Alpha-diversity of microbial taxa. Box-plots represent α-diversity metrics: Pielou's evenness, Faith's phylogenetic diversity, Shannon's index, and Simpson's index. **p < 0.01, ***p < 0.005, and ****p < 0.001 compared to the DON 0 group as determined by the Kruskal-Wallis pairwise test. (B) Principal coordinate analysis plots representing the β-diversity for unweighted Unifrac distance and Bray-Curtis dissimilarity. Red dots = DON 0, blue dots = DON 10, and orange dots = DON 100 groups. (C) Differential abundance of significantly changed bacterial orders. (D) Differential abundance of significantly changed bacterial families. (E) Differential abundance of significantly changed bacterial genera. For (C–E), * indicates bacteria which reject the null hypothesis >95 % with ANCOM.

abundant in the 10 μg DON group; *Peptococcaceae* and *Defluviitaleaceae* were more abundant in the 100 μg DON group (Fig. 6D); and *Helicobacteraceae* was significantly enriched in mice from both DON treatment groups. At the genus level, the *Eubacterium ruminantium* group, *Coriobacteriaceae UCG-002*, and *Papillibacter* were found to be more abundant in the 10 μg DON group, and *Anaeroplasma* was less abundant in the 100 μg DON group (Fig. 6E). Most notably, the relative abundance of *Fournierella* and *Dubosiella* genera were respectively higher and lower after exposure to10 and 100 μg/kg bw/day of DON. The two latter genera, as well as all the orders and families detected as significantly different with ANCOM, were also verified with corncob.

3.5. Functional gene analysis

The bioinformatic software package PICRUSt2 was used to predict the MetaCyc pathways of microbiota and the significantly changed MetaCyc pathways are shown in Fig. 7A. Six pathways were enriched in the control CRC group compared with the 100 μg DON group, including the superpathway of methanogenesis from acetate (METH-ACETATE-PWY; effect size −1.8; $p = 0.02$) and two pathways related to toluene degradation (PWY-5182 and PWY-5180; effect size −1.1; $p = 0.01$ for both). Twelve Metacyc pathways were identified as enriched in DON-exposed mice. Among them, three were related to fucose and rhamnose degradation (FUC-RHAMCAT-PWY, RHAMCAT-PWY, and FUCCAT-PWY; effect sizes 3, 2.6, and 2.3 respectively; $p = 0.001$). The pathway with highest enrichment, the superpathway of fucose and rhamnose degradation enzymes (FUC-RHAMCAT-PWH), was three-fold more abundant in the 100 μg DON group compared with the control CRC group ($p < 0.001$; Suppl Fig. 5A).

Most of the functional genes of the superpathway of fucose and rhamnose degradation enzymes were much more abundant in DON-exposed microbiota (Fig. 7B). Genes encoding three out of the 4 enzymes involved in the transformation of β- L-fucose to (*S*)-lactaldehyde, namely L-fucose mutarotase (FucU), L-fucose isomerase (FucI), and L-fuculokinase (Fuck), were underrepresented; and L-fuculose-phosphate aldolase (FucA) did not vary. DON exposure also increased the relative abundance of all genes associated with the transformation of α-L-rhamnopyranose to (*S*)-lactaldehyde, including L-rhamnose mutarotase (RhaM), L-rhamnose isomerase (RhaA), rhamnulokinase (RhaB) and rhamnulose-1-phosphate aldolase (RhaD). Suppl Fig. 5B shows the bacterial genera which were significantly associated with the relative abundance of FUC-RHAMCAT-PWH. Twenty-five genera were positively associated with FUC-RHAMCAT-PWH, with *Ruminococcus UCG-014* presenting the highest positive correlation level (Spearman rho 0.8872; 95 % CI 0.7184 to 0.9574; $p < 0.0001$). Eleven genera were negatively associated, with *Ruminiclostridium* presenting the highest negative correlation (Spearman rho −0.8018; 95 % CI 0.9229 to −0.5364; $p < 0.0001$).

3.6. Effect of DON on microbiota fucose and rhamnose metabolism

To further explore the increased fucose and rhamnose degradation

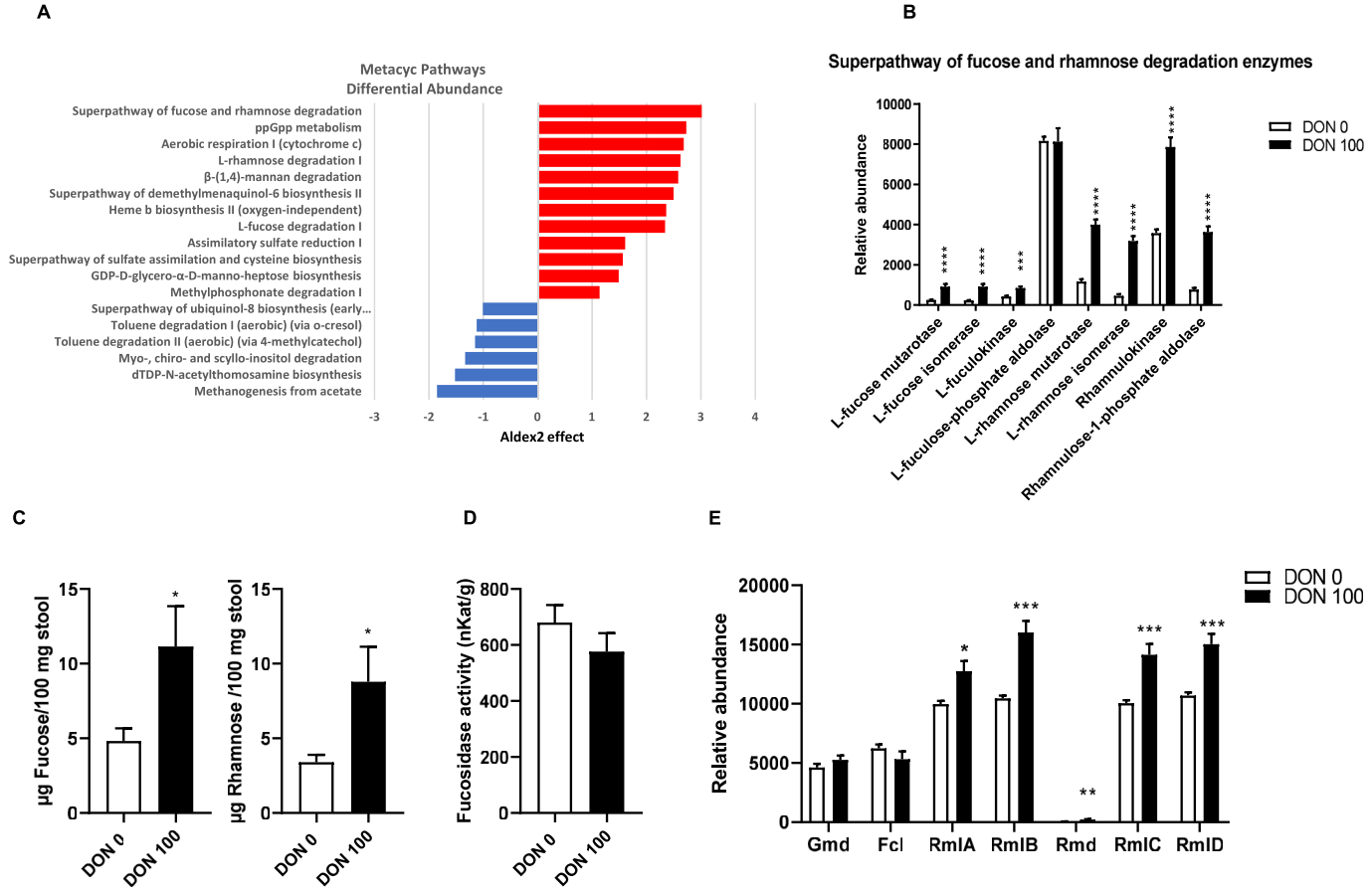

Fig. 7. Effects of deoxynivalenol (DON) exposure on microbiota fucose and rhamnose metabolism in mice with colorectal cancer. (A-B) Predicted Metacyc pathways in mice with colorectal cancer unexposed or exposed to deoxynivalenol (DON) (100 μg/kg bw/day). (A) Differential abundance of significantly changed Metacyc pathways. $p \leq 0.01$ as determined by the Wilcoxon test. (B) Relative abundance of genes constituting the superpathway of fucose and rhamnose degradation enzymes. (C) Fucose and rhamnose levels within stool. (D) Stool fucosidase activity. (E) Relative abundance of genes involved in eukaryotic fucose incorporation (Gmd and Fcl) and. in fucose and rhamnose biosynthesis (RmlA, RmlB, Rmd, RmlC, RmlD). *p < 0.05, **p < 0.01, ***p < 0.005, and ****p < 0.001 compared to the control group as determined by the Mann-Whitney U test.

induced in microbiota by DON exposure, we quantified fucose and rhamnose content in mouse stool by GC/MS (Fig. 7C). The levels of luminal fucose and rhamnose were significantly higher in DON-exposed CRC mice than in the control CRC mice. Microbiota fucosidase activity was measured to determine whether this was causing an increase in these sugars. Luminal fucosidase activities were similar between DON-exposed CRC mice and control CRC mice (Fig. 7D).

Next, genes associated with the incorporation of fucose into eukaryotic glycoproteins, glycolipids, and bacterial polysaccharides, specifically GDP-mannose 4,6-dehydratase Gmd and GDP-L-fucose synthetase Fcl were assayed and found to be unmodified by DON exposure (Fig. 7E) (Coyne et al., 2005). Two genes involved in the common first steps of fucose and rhamnose biosynthesis, glucose-1-phosphate thymidylyltransferase RmlA and dTDP-glucose 4,6-dehydratase RmlB, had higher expression in DON-exposed CRC mice relative to control CRC mice. Genes involved in fucose biosynthesis, such as dTDP-4-dehydro-6-deoxyglucose reductase Fcd and dTDP-fucopyranose mutase Fcf2, were not found in the PICRUSt2 data. But genes associated with rhamnose biosynthesis were more abundant in DON-exposed mice. Indeed, GDP-4-dehydro-6-deoxy-D-mannose reductase Rmd involved with biosynthesis of GDP-D-Rhamnose, as well as dTDP-4-dehydrorhamnose 3,5-epimerase RmlC and dTDP-4-dehydrorhamnose reductase RmlD, involved with biosynthesis of dTDP-L-Rhamnose, were overrepresented in microbiota of DON-exposed CRC mice. Overall, the increased levels of luminal fucose and rhamnose and the overrepresentation of genes associated with both degradation and biosynthesis of these sugars show that chronic DON exposure led to worse outcomes in an AOM-DSS-induced colorectal cancer model which was associated with altered microbiotic fucose and rhamnose metabolism.

3.7. Correlation between gut microbiota and colorectal cancer markers

To further analyze the relationship between gut microbiota and colorectal cancer development, the correlations between the changed gut microbiota and measured AOM-DSS colorectal cancer variables were explored by Spearman's correlation analysis and presented by a heatmap (Fig. 8). The results from the order-level analysis showed that the change in abundance of *Anaeroplasmatales* was negatively correlated with the mRNA levels of a majority of ERK signaling genes. The abundance of *Campylobacterales* was inversely positively correlated with ERK signaling genes, as well as with histological colitis parameters. The results revealed strong negative correlations between the abundance of *Anaeroplasmataceae* family and most of ERK signaling genes. There were similar correlations for the *Peptococcaceae* family, which was also negatively associated with several parameters of colon inflammation. The two other families, *Defluvitaleaceae* and *Helicobacteraceae*, were positively associated with ERK signaling gene levels. Moreover, both families showed positive correlations with colitis parameters, and *Defluvitaleaceae* abundance was positively associated with medium and high tumor count and hyperplasia score. Four bacterial genera were positively correlated with several ERK signaling gene levels, *Eubacterium ruminatium group*, *Coriobacteriaceae UCG-002 group*, *Papillibacter*, and *Fournierella*. These last two genera were also positively correlated with several inflammation parameters. In addition, *Eubacterium ruminantium group* abundance was positively correlated with three tumorigenesis parameters. The results also revealed significant negative correlations between the *Anaeroplasma* and *Dubosiella* genera and ERK signaling gene expression. Most importantly, these analyses showed strong negative correlations between *Dubosiella* abundance and a majority of colitis and tumorigenesis parameters. Furthermore, Mapk1, Mapk3, Map2k1, Map2k2, Bcl2 and Bcl2l1 transcript levels were significantly correlated with 11/12 bacterial strain abundance, showing a close relationship

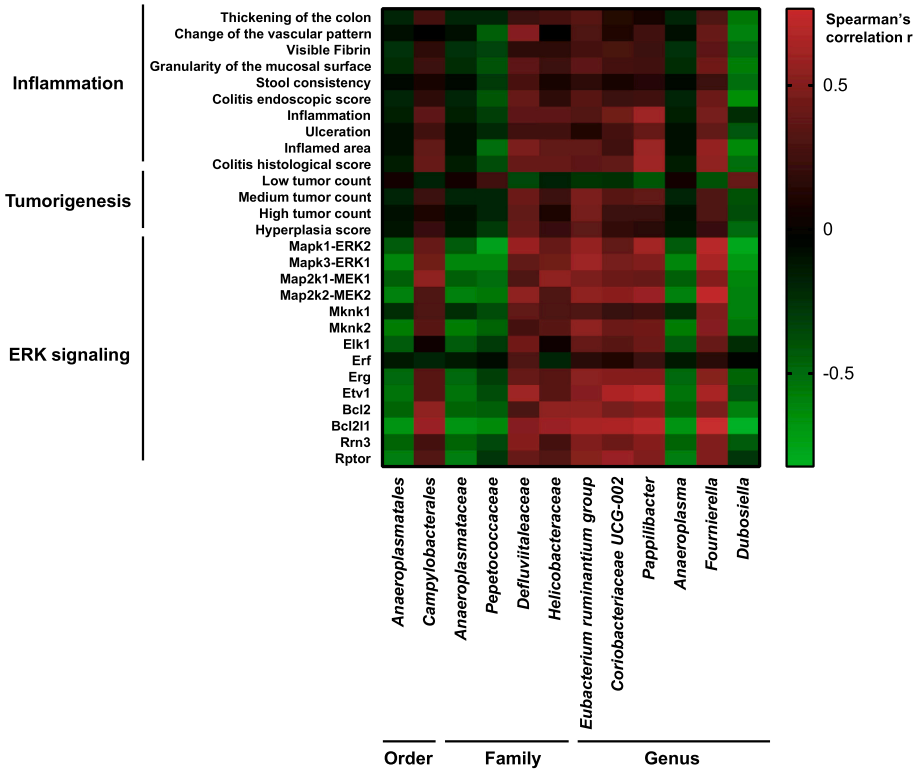

Fig. 8. Heatmap of Spearman's rank correlation between the abundance of the changed gut microbiota and colon inflammation, tumorigenesis and ERK signaling variables measured in mice with colorectal cancer unexposed or exposed to deoxynivalenol (DON) (100 μg/kg bw/day). *p < 0.05, **p < 0.01, ***p < 0.005, and ****$p < 0.001$.

between gut microbiota variation and ERK signaling in DON-induced worsening of colorectal cancer.

4. Discussion

In this study, we explored the impact of DON exposure in murine models at doses relevant to human exposure. For deoxynivalenol, JECFA (joint FAO/WHO expert committee on food additives) set the tolerable daily intake at 1 μg/kg bw/day (Knutsen et al., 2017). The translation from humans to animals using the body surface area normalization method gives the dose of 12 μg/kg bw/day (Reagan-Shaw et al., 2008). Besides, in the assessment of DON exposure by EFSA CONTAM panel (European Food Safety Authority panel on Contaminants in the Food Chain) performed across 39 different dietary surveys and all age groups, the 95th percentile acute exposure ranged from 0.7 to 6.7 μg/kg bw/day. Their translation to mouse gives doses of 8.6 to 83 μg/kg bw/day. Therefore, we selected 10 and 100 μg/kg bw/day as representative doses of realistic human exposure. These concentrations are much lower than those commonly used in the literature (Grenier and Applegate, 2013), and allowed us to assess the toxicity of DON closer to human exposure conditions. At both dosages after 8 days of exposure, a significant increase in intestinal epithelial cell proliferation was observed as evidenced by enhanced crypt length and PCNA staining in ileum, jejunum, and duodenum of mice. A similar increase in intestinal epithelial proliferation has been described in mice jejunum following longer exposure conditions (9 months) or at a higher concentration (2 mg/kg bw/day) (Vignal et al., 2018; Zhou et al., 2019). An increase of crypt depth has been shown in piglet jejunum and duodenum after 10 days exposure at 0.9 mg/kg of feed (Alizadeh et al., 2015) and in pig jejunum after 6 weeks exposure at 12 μg/kg bw/day (Przybylska-Gornowicz et al., 2015). Data from the literature have described an increase of epithelial proliferation in protocols with exposure times at least 5 times longer or with exposure concentrations 9 to 200 times higher. Thus, our assessment of DON toxicity, which is closer to human exposure conditions, highlights the risks associated with short-term intake of even low levels of this toxin.

Concerning effects of DON ingestion on the small intestine, short-term intoxication was found to exacerbate the severity of indomethacin-induced enteritis. DON ingestion has been shown to predispose broiler chickens to the development of an infectious model of enteritis (induced by *Clostridium perfringens*) (Antonissen et al., 2014). Moreover, dietary contamination with DON (8 mg/kg of food for 4 weeks) increased the severity of colon injury in a rat model of DSS-induced colitis (Payros et al., 2020). More recently, a 28-day exposure to 25 and 50 μg/kg bw/day of DON aggravated colitis in C57BL/6 mice, which is consistent with our data (Gan et al., 2023). Cumulatively, these data suggest that DON exposure has the potential to aggravate any pre-existing inflammatory condition in small intestine, regardless of its origin. Therefore, the involvement of DON in the development of infectious and food-allergic enteritis, appendicitis, peptic ulcers, and inflammatory bowel diseases deserves more investigation.

In addition to inflammatory conditions, here we showed that DON exposure can also enhance carcinogenesis *in vivo* in the AOM-DSS-induced model of colorectal cancer. A deep analysis of cecal microbiota diversity, structure, and function was performed to better understand how DON exposure can alter microbial pathways and possibly affect CRC promotion. The α-diversity metric, which describes the relative number of bacterial taxa, was greater in DON-exposed mice compared to controls. Moreover, the β-diversity indices indicated strong differences in microbiotic composition between the three groups of mice. This variability was mainly attributable to a small subgroup of bacterial taxa. The most notable effect was increased relative abundance of the *Campylobacterales* order in both DON exposure groups, which includes the *Helicobacteraceae* family. Although *Helicobacter hepaticus* has been shown to promote AOM-initiated colon tumorigenesis (Nagamine et al., 2008), our analysis did not show significant variation of this strain.

The results of the Spearman's correlation analysis globally show strong correlations between the modified bacteria and the variables characterizing colorectal cancer, what further argues in favor of an important role of intestinal microbiota in the protumorigenic effects of DON. The overabundance of *Eubacterium ruminantium group*, *Coriobacteriaceae UCG-002*, *Papillibacter* and *Fournierella*, as well as the underabundance of *Anaeroplasma* and *Dubiosiella* may contribute to DON-induced CRC exacerbation. Particularly, our findings showing negative correlations between most of the measured variables and the abundance of *Dubosiella* suggest that the defect of this strain could be an important contributing mechanism to the worsening effect of DON in the AOM-DSS model.

PICRUSt2 analysis showed dysregulation of several microbiotic gene pathways in mice exposed to DON, including those associated with the degradation of fucose. These results are consistent with a previous study which showed a decreasing trend of the relative abundance of the fucose fraction within intestinal mucin oligosaccharide profiles of broiler chicken duodenum exposed to a DON-contaminated diet (Antonissen et al., 2015). In the mammalian gastrointestinal tract, fucose is an abundant component of glycans that decorate proteins and lipids, especially on the lumen-facing epithelial surface and in mucosal secretions (Pickard and Chervonsky, 2015). Fucosylated proteins are shed into the lumen and fucose is liberated and metabolized by diverse gut microbiota (Bocci and Winzler, 1969). Many symbiotic gut bacteria species can and do use fucose, and it has been found to be protective in several disease models, such as on commensal bacteria in cases of intestinal pathogen infection (Garber et al., 2021; Pickard et al., 2014). Fucose can ameliorate intestinal inflammation, as exogenous administration of fucose has been shown to inhibit chronic colitis development in mice (Ke et al., 2020). Furthermore, L-rhamnose and L-fucose can suppress cancer growth in mice (Tomsik et al., 2011), and host fucosylation deficiency in mice led to colitis and adenocarcinoma (Wang et al., 2017). Therefore, it can be hypothesized that the dysregulation of fucose and rhamnose metabolism in DON-exposed mice may be a mechanism that potentiates colorectal tumorigenesis.

Other potential mechanisms can also participate in the protumorigenic effect of DON such as increasing the carcinogenic potential of genotoxins present in the diet or in the microbiota. For example, in the non-transformed intestinal epithelial cell line IEC-6, DON is not genotoxic on its own but aggravates DNA damage induced by a broad spectrum of genotoxic agents such as etoposide, cisplatin, and phleomycin (Garofalo et al., 2022). In addition, dietary contamination with DON increased intestinal DNA damage in rats colonized with *E. coli* which produce colibactin - a polyketide peptide which can alkylate DNA (Payros et al., 2017).

5. Conclusion

Epithelial cell proliferation was increased in duodenum, jejunum, ileum, and colon in mice after 8-day exposure to DON at a dose which is translational to human dietary exposure. DON exposure also led to exacerbation of indomethacin-induced enteritis intensity and colorectal carcinogenesis development in murine model systems. The protumorigenic effect of DON was associated with altered gut microbiota diversity, composition, and metabolism of fucose and rhamnose.

This study adds to our knowledge of the harmful effects of DON in the gut and highlights the need to pay particular attention to individuals with intestinal susceptibility. More studies are required to better characterize the effects of DON ingestion on the development of colorectal cancer, and to assess the relevance of these effects in humans.

Authors' contribution

MBM and MD performed the study conceptualization. Fucose and rhamnose measurements by GC/MS were performed by KL. Fucosidase

activity assay was performed by AS and M S.D. SC, DB and DH performed microbiota analyses. Other experiments, data collection, and analyses were performed by MD, CW, MBM, and CV. MD developed endoscopy methodology. CV, LD, and DL contributed to supervision and funding acquisition. The draft of the manuscript was written by MBM. All authors read and approved the final manuscript.

Funding

This work was supported by a grant from the FHU Imminent and a grant from the French National Research Agency (ANR EVICTION).

Ethics approval

All animal procedures were approved by the regional Animal Experimentation Ethics Committee (Comité d'Ethique en Expérimentation Animale, Hauts-de-France, CEEA 75) and the French Ministry of Higher Education and Research (Ministère de l'Enseignement Supérieur et de la Recherche) (authorization numbers: APAFIS #9249-2017031312157794 and 2020071610201738). Mice received human care in compliance with European animal welfare regulations (European Communities Council Directive of 1986 revised in 2010, 2010/63/EU).

Declaration of competing interest

The authors declare no competing financial interest.

Data availability

Data will be made available on request.

Acknowledgments

The authors thank Thomas Hubert and the staff of the animal facilities of Lille University Hospital (DHURE & EOPS). We are grateful to Bernadette Leu for her excellent broad range of help. Editorial assistance, in the form of language editing and correction, was provided by XpertScientific Editing and Consulting Services.

Appendix A. Supplementary data

Supplementary data to this article can be found online at https://doi.org/10.1016/j.scitotenv.2023.165722.

References

Alizadeh, A., Braber, S., Akbari, P., Garssen, J., Fink-Gremmels, J., 2015. Deoxynivalenol impairs weight gain and affects markers of gut health after low-dose, short-term exposure of growing pigs. Toxins 7, 2071–2095. https://doi.org/10.3390/toxins7062071.

Antonissen, G., Immerseel, F.V., Pasmans, F., Ducatelle, R., Haesebrouck, F., Timbermont, L., Verlinden, M., Janssens, G.P.J., Eeckhaut, V., Eeckhout, M., Saeger, S.D., Hessenberger, S., Martel, A., Croubels, S., 2014. The mycotoxin deoxynivalenol predisposes for the development of clostridium perfringens-induced necrotic enteritis in broiler chickens. PLoS One 9, e108775. https://doi.org/10.1371/journal.pone.0108775.

Antonissen, G., Van Immerseel, F., Pasmans, F., Ducatelle, R., Janssens, G.P.J., De Baere, S., Mountzouris, K.C., Su, S., Wong, E.A., De Meulenaer, B., Verlinden, M., Devreese, M., Haesebrouck, F., Novak, B., Dohnal, I., Martel, A., Croubels, S., 2015. Mycotoxins deoxynivalenol and fumonisins alter the extrinsic component of intestinal barrier in broiler chickens. J. Agric. Food Chem. 63, 10846–10855. https://doi.org/10.1021/acs.jafc.5b04119.

Becker, C., Fantini, M.C., Wirtz, S., Nikolaev, A., Kiesslich, R., Lehr, H.A., Galle, P.R., Neurath, M.F., 2005. In vivo imaging of colitis and colon cancer development in mice using high resolution chromoendoscopy. Gut 54, 950–954. https://doi.org/10.1136/gut.2004.061283.

Bocci, V., Winzler, R.J., 1969. Metabolism of L-fucose-1-14C and of fucose glycoproteins in the rat. Am. J. Phys. 216, 1337–1342. https://doi.org/10.1152/ajplegacy.1969.216.6.1337.

Body-Malapel, M., Djouina, M., Waxin, C., Langlois, A., Gower-Rousseau, C., Zerbib, P., Schmidt, A.-M., Desreumaux, P., Boulanger, E., Vignal, C., 2019. The RAGE signaling pathway is involved in intestinal inflammation and represents a promising therapeutic target for inflammatory bowel diseases. Mucosal Immunol. 12, 468–478. https://doi.org/10.1038/s41385-018-0119-z.

Bolyen, E., Rideout, J.R., Dillon, M.R., Bokulich, N.A., Abnet, C.C., Al-Ghalith, G.A., Alexander, H., Alm, E.J., Arumugam, M., Asnicar, F., Bai, Y., Bisanz, J.E., Bittinger, K., Brejnrod, A., Brislawn, C.J., Brown, C.T., Callahan, B.J., Caraballo-Rodríguez, A.M., Chase, J., Cope, E.K., Da Silva, R., Diener, C., Dorrestein, P.C., Douglas, G.M., Durall, D.M., Duvallet, C., Edwardson, C.F., Ernst, M., Estaki, M., Fouquier, J., Gauglitz, J.M., Gibbons, S.M., Gibson, D.L., Gonzalez, A., Gorlick, K., Guo, J., Hillmann, B., Holmes, S., Holste, H., Huttenhower, C., Huttley, G.A., Janssen, S., Jarmusch, A.K., Jiang, L., Kaehler, B.D., Kang, K.B., Keefe, C.R., Keim, P., Kelley, S.T., Knights, D., Koester, I., Kosciolek, T., Kreps, J., Langille, M.G.I., Lee, J., Ley, R., Liu, Y.-X., Loftfield, E., Lozupone, C., Maher, M., Marotz, C., Martin, B.D., McDonald, D., McIver, L.J., Melnik, A.V., Metcalf, J.L., Morgan, S.C., Morton, J.T., Naimey, A.T., Navas-Molina, J.A., Nothias, L.F., Orchanian, S.B., Pearson, T., Peoples, S.L., Petras, D., Preuss, M.L., Pruesse, E., Rasmussen, L.B., Rivers, A., Robeson, M.S., Rosenthal, P., Segata, N., Shaffer, M., Shiffer, A., Sinha, R., Song, S.J., Spear, J.R., Swafford, A.D., Thompson, L.R., Torres, P.J., Trinh, P., Tripathi, A., Turnbaugh, P.J., Ul-Hasan, S., van der Hooft, J.J.J., Vargas, F., Vázquez-Baeza, Y., Vogtmann, E., von Hippel, M., Walters, W., Wan, Y., Wang, M., Warren, J., Weber, K. C., Williamson, C.H.D., Willis, A.D., Xu, Z.Z., Zaneveld, J.R., Zhang, Y., Zhu, Q., Knight, R., Caporaso, J.G., 2019. Reproducible, interactive, scalable and extensible microbiome data science using QIIME 2. Nat. Biotechnol. 37, 852–857. https://doi.org/10.1038/s41587-019-0209-9.

Callahan, B.J., McMurdie, P.J., Rosen, M.J., Han, A.W., Johnson, A.J.A., Holmes, S.P., 2016. DADA2: high-resolution sample inference from Illumina amplicon data. Nat. Methods 13, 581–583. https://doi.org/10.1038/nmeth.3869.

Chen, C., Turna, N.S., Wu, F., 2019. Risk assessment of dietary deoxynivalenol exposure in wheat products worldwide: are new codex DON guidelines adequately protective? Trends Food Sci. Technol. 89, 11–25. https://doi.org/10.1016/j.tifs.2019.05.002.

Coyne, M.J., Reinap, B., Lee, M.M., Comstock, L.E., 2005. Human symbionts use a host-like pathway for surface fucosylation. Science 307, 1778–1781.

Davis, N.M., Proctor, D.M., Holmes, S.P., Relman, D.A., Callahan, B.J., 2018. Simple statistical identification and removal of contaminant sequences in marker-gene and metagenomics data. Microbiome 6, 226. https://doi.org/10.1186/s40168-018-0605-2.

De Ruyck, K., De Boevre, M., Huybrechts, I., De Saeger, S., 2015. Dietary mycotoxins, co-exposure, and carcinogenesis in humans: short review. Mutat. Res. Rev. Mutat. Res. 766, 32–41. https://doi.org/10.1016/j.mrrev.2015.07.003.

Douglas, G.M., Maffei, V.J., Zaneveld, J.R., Yurgel, S.N., Brown, J.R., Taylor, C.M., Huttenhower, C., Langille, M.G., 2020. PICRUSt2 for prediction of metagenome functions. Nat. Biotechnol. 38, 685–688.

Fernandes, A.D., Reid, J.N., Macklaim, J.M., McMurrough, T.A., Edgell, D.R., Gloor, G.B., 2014. Unifying the analysis of high-throughput sequencing datasets: characterizing RNA-seq, 16S rRNA gene sequencing and selective growth experiments by compositional data analysis. Microbiome 2, 1–13.

Gan, F., Lin, Z., Tang, J., Chen, X., Huang, K., 2023. Deoxynivalenol at no-observed adverse-effect levels aggravates DSS-induced colitis through the JAK2/STAT3 signaling pathway in mice. J. Agric. Food Chem. https://doi.org/10.1021/acs.jafc.3c00252.

Garber, J.M., Hennet, T., Szymanski, C.M., 2021. Significance of fucose in intestinal health and disease. Mol. Microbiol. 115, 1086–1093. https://doi.org/10.1111/mmi.14681.

Garofalo, M., Payros, D., Oswald, E., Nougayrède, J.-P., Oswald, I.P., 2022. The foodborne contaminant deoxynivalenol exacerbates DNA damage caused by a broad spectrum of genotoxic agents. Sci. Total Environ. 820, 153280 https://doi.org/10.1016/j.scitotenv.2022.153280.

Grenier, B., Applegate, T.J., 2013. Modulation of intestinal functions following mycotoxin ingestion: meta-analysis of published experiments in animals. Toxins 5, 396–430. https://doi.org/10.3390/toxins5020396.

Hooft, J.M., Bureau, D.P., 2021. Deoxynivalenol: mechanisms of action and its effects on various terrestrial and aquatic species. Food Chem. Toxicol. 157, 112616 https://doi.org/10.1016/j.fct.2021.112616.

Kamle, M., Mahato, D.K., Gupta, A., Pandhi, S., Sharma, B., Dhawan, K., Vasundhara, Mishra, S., Kumar, M., Tripathi, A.D., 2022. Deoxynivalenol: an overview on occurrence, chemistry, biosynthesis, health effects and its detection, management, and control strategies in food and feed. Microbiol. Res. 13, 292–314.

Ke, J., Li, Y., Han, C., He, R., Lin, R., Qian, W., Hou, X., 2020. Fucose ameliorate intestinal inflammation through modulating the crosstalk between bile acids and gut microbiota in a chronic colitis murine model. Inflamm. Bowel Dis. 26, 863–873. https://doi.org/10.1093/ibd/izaa007.

Knutsen, H.K., Alexander, J., Barregård, L., Bignami, M., Brüschweiler, B., Ceccatelli, S., Cottrill, B., Dinovi, M., Grasl-Kraupp, B., Hogstrand, C., Hoogenboom, L. (Ron), Nebbia, C.S., Oswald, I.P., Petersen, A., Rose, M., Roudot, A.-C., Schwerdtle, T., Vleminckx, C., Vollmer, G., Wallace, H., Saeger, S.D., Eriksen, G.S., Farmer, P., Fremy, J.-M., Gong, Y.Y., Meyer, K., Naegeli, H., Parent-Massin, D., Rietjens, I., van Egmond, H., Altieri, A., Eskola, M., Gergelova, P., Bordajandi, L.R., Benkova, B., Dörr, B., Gkrillas, A., Gustavsson, N., van Manen, M., Edler, L., 2017. Risks to human and animal health related to the presence of deoxynivalenol and its acetylated and modified forms in food and feed. EFSA J. 15, e04718 https://doi.org/10.2903/j.efsa.2017.4718.

Lavoie, H., Gagnon, J., Therrien, M., 2020. ERK signalling: a master regulator of cell behaviour, life and fate. Nat. Rev. Mol. Cell Biol. 21, 607–632. https://doi.org/10.1038/s41580-020-0255-7.

Lee, J.-Y., Lim, W., Park, S., Kim, J., You, S., Song, G., 2019. Deoxynivalenol induces apoptosis and disrupts cellular homeostasis through MAPK signaling pathways in

bovine mammary epithelial cells. Environ. Pollut. 252, 879–887. https://doi.org/10.1016/j.envpol.2019.06.001.
Liao, Y., Peng, Z., Chen, L., Nüssler, A.K., Liu, L., Yang, W., 2018. Deoxynivalenol, gut microbiota and immunotoxicity: a potential approach? Food Chem. Toxicol. 112, 342–354. https://doi.org/10.1016/j.fct.2018.01.013.
Liu, M., Zhang, L., Mo, Y., Li, J., Yang, J., Wang, J., Karrow, N.A., Wu, H., Sun, L., 2023. Ferroptosis is involved in deoxynivalenol-induced intestinal damage in pigs. J. Anim. Sci. Biotechnol. 14, 29. https://doi.org/10.1186/s40104-023-00841-4.
Livak, K.J., Schmittgen, T.D., 2001. Analysis of relative gene expression data using real-time quantitative PCR and the 2- ΔΔCT method. Methods 25, 402–408. https://doi.org/10.1006/meth.2001.1262.
Mandal, S., Van Treuren, W., White, R.A., Eggesbø, M., Knight, R., Peddada, S.D., 2015. Analysis of composition of microbiomes: a novel method for studying microbial composition. Microb. Ecol. Health Dis. 26, 27663.
Martin, B.D., Witten, D., Willis, A.D., 2020. Modeling microbial abundances and dysbiosis with beta-binomal regression. Ann. Appl. Stat. 14, 94–115. https://doi.org/10.1214/19-aoas1283.
Nagamine, C.M., Rogers, A.B., Fox, J.G., Schauer, D.B., 2008. Helicobacter hepaticus promotes azoxymethane-initiated colon tumorigenesis in BALB/c-IL10-deficient mice. Int. J. Cancer 122, 832–838. https://doi.org/10.1002/ijc.23175.
Payros, D., Dobrindt, U., Martin, P., Secher, T., Bracarense, A.P.F.L., Boury, M., Laffitte, J., Pinton, P., Oswald, E., Oswald, I.P., 2017. The food contaminant deoxynivalenol exacerbates the genotoxicity of gut microbiota. mBio 8. https://doi.org/10.1128/mBio.00007-17.
Payros, D., Ménard, S., Laffitte, J., Neves, M., Tremblay-Franco, M., Luo, S., Fouche, E., Snini, S.P., Theodorou, V., Pinton, P., Oswald, I.P., 2020. The food contaminant, deoxynivalenol, modulates the Thelper/Treg balance and increases inflammatory bowel diseases. Arch. Toxicol. https://doi.org/10.1007/s00204-020-02817-z.
Phan, T., Zhang, X.H., Rosen, S., Melstrom, L.G., 2023. P38 kinase in gastrointestinal cancers. Cancer Gene Ther. 1–9 https://doi.org/10.1038/s41417-023-00622-1.
Pickard, J.M., Chervonsky, A.V., 2015. Intestinal fucose as a mediator of host–microbe symbiosis. J. Immunol. 194, 5588–5593. https://doi.org/10.4049/jimmunol.1500395.
Pickard, J.M., Maurice, C.F., Kinnebrew, M.A., Abt, M.C., Schenten, D., Golovkina, T.V., Bogatyrev, S.R., Ismagilov, R.F., Pamer, E.G., Turnbaugh, P.J., Chervonsky, A.V., 2014. Rapid fucosylation of intestinal epithelium sustains host–commensal symbiosis in sickness. Nature 514, 638–641. https://doi.org/10.1038/nature13823.
Pinton, P., Braicu, C., Nougayrede, J.-P., Laffitte, J., Taranu, I., Oswald, I.P., 2010. Deoxynivalenol impairs porcine intestinal barrier function and decreases the protein expression of Claudin-4 through a mitogen-activated protein kinase-dependent mechanism. J. Nutr. 140, 1956–1962. https://doi.org/10.3945/jn.110.123919.
Przybylska-Gornowicz, B., Tarasiuk, M., Lewczuk, B., Prusik, M., Ziółkowska, N., Zielonka, Ł., Gajęcki, M., Gajęcka, M., 2015. The effects of low doses of two fusarium toxins, Zearalenone and deoxynivalenol, on the pig jejunum. A light and electron microscopic study. Toxins 7, 4684–4705. https://doi.org/10.3390/toxins7114684.
Reagan-Shaw, S., Nihal, M., Ahmad, N., 2008. Dose translation from animal to human studies revisited. FASEB. J. Off. Publ. Fed. Am. Soc. Exp. Biol. 22, 659–661. https://doi.org/10.1096/fj.07-9574LSF.
Steimle, A., Grant, E.T., Desai, M.S., 2021. Quantitative assay to detect bacterial glycan-degrading enzyme activities in mouse and human fecal samples. STAR Protoc. 2, 100326 https://doi.org/10.1016/j.xpro.2021.100326.
Tardivel, C., Airault, C., Djelloul, M., Guillebaud, F., Barbouche, R., Troadec, J.-D., Gaige, S., Dallaporta, M., 2015. The food born mycotoxin deoxynivalenol induces low-grade inflammation in mice in the absence of observed-adverse effects. Toxicol. Lett. 232, 601–611.
Tomsik, P., Soukup, T., Cermakova, E., Micuda, S., Niang, M., Sucha, L., Rezacova, M., 2011. L-rhamnose and L-fucose suppress cancer growth in mice. Cent. Eur. J. Biol. 6, 1–9. https://doi.org/10.2478/s11535-010-0087-0.
Vignal, C., Djouina, M., Pichavant, M., Caboche, S., Waxin, C., Beury, D., Hot, D., Gower-Rousseau, C., Body-Malapel, M., 2018. Chronic ingestion of deoxynivalenol at human dietary levels impairs intestinal homeostasis and gut microbiota in mice. Arch. Toxicol. 92, 2327–2338. https://doi.org/10.1007/s00204-018-2228-6.
Wang, Y., Huang, D., Chen, K.-Y., Cui, M., Wang, W., Huang, X., Awadellah, A., Li, Q., Friedman, A., Xin, W.W., Martino, L.D., Cominelli, F., Miron, A., Chan, R., Fox, J.G., Xu, Y., Shen, X., Kalady, M.F., Markowitz, S., Maillard, I., Lowe, J.B., Xin, W., Zhou, L., 2017. Fucosylation deficiency in mice leads to colitis and adenocarcinoma. Gastroenterology 152, 193–205.e10. https://doi.org/10.1053/j.gastro.2016.09.004.
Wang, X., Fan, M., Chu, X., Zhang, Y., Rahman, S. ur, Jiang, Y., Chen, X., Zhu, D., Feng, S., Li, Y., Wu, J., 2018. Deoxynivalenol induces toxicity and apoptosis in piglet hippocampal nerve cells via the MAPK signaling pathway. Toxicon 155, 1–8. https://doi.org/10.1016/j.toxicon.2018.09.006.
Wang, L., Liao, Y., Peng, Z., Chen, L., Zhang, W., Nüssler, A.K., Shi, S., Liu, L., Yang, W., 2019. Food raw materials and food production occurrences of deoxynivalenol in different regions. Trends Food Sci. Technol. 83, 41–52. https://doi.org/10.1016/j.tifs.2018.11.003.
Wang, S., Wu, K., Xue, D., Zhang, C., Rajput, S.A., Qi, D., 2021. Mechanism of deoxynivalenol mediated gastrointestinal toxicity: insights from mitochondrial dysfunction. Food Chem. Toxicol. 153, 112214.
Wang, J., Sijs, B., Bakker, W., de Haan, L., Bouwmeester, H., 2023. Ribotoxin deoxynivalenol induces taurocholic acid malabsorption in an in vitro human intestinal model. Toxicol. Lett. 383, 54–63. https://doi.org/10.1016/j.toxlet.2023.06.001.
Woelflingseder, L., Warth, B., Vierheilig, I., Schwartz-Zimmermann, H., Hametner, C., Nagl, V., Novak, B., Šarkanj, B., Berthiller, F., Adam, G., Marko, D., 2019. The fusarium metabolite culmorin suppresses the in vitro glucuronidation of deoxynivalenol. Arch. Toxicol. 93, 1729–1743. https://doi.org/10.1007/s00204-019-02459-w.
Xiao, X., Nakatsu, G., Jin, Y., Wong, S., Yu, J., Lau, J.Y.W., 2017. Gut microbiota mediates protection against enteropathy induced by indomethacin. Sci. Rep. 7, 40317. https://doi.org/10.1038/srep40317.
Yang, J., Wang, J., Guo, W., Ling, A., Luo, A., Liu, D., Yang, X., Zhao, Z., 2019. Toxic effects and possible mechanisms of deoxynivalenol exposure on sperm and testicular damage in BALB/c mice. J. Agric. Food Chem. 67, 2289–2295. https://doi.org/10.1021/acs.jafc.8b04783.
You, L., Zhao, Y., Kuca, K., Wang, X., Oleksak, P., Chrienova, Z., Nepovimova, E., Jaćević, V., Wu, Q., Wu, W., 2021. Hypoxia, oxidative stress, and immune evasion: a trinity of the trichothecenes T-2 toxin and deoxynivalenol (DON). Arch. Toxicol. 95, 1899–1915. https://doi.org/10.1007/s00204-021-03030-2.
Zaki, M.H., Vogel, P., Body-Malapel, M., Lamkanfi, M., Kanneganti, T.-D., 2010. IL-18 production downstream of the Nlrp3 inflammasome confers protection against colorectal tumor formation. J. Immunol. Baltim. Md 1950 (185), 4912–4920. https://doi.org/10.4049/jimmunol.1002046.
Zhang, Hua, Deng, X., Zhou, C., Wu, W., Zhang, Haibin, 2020. Deoxynivalenol induces inflammation in IPEC-J2 cells by activating P38 Mapk and Erk1/2. Toxins 12, 180. https://doi.org/10.3390/toxins12030180.
Zhao, L., Zhang, L., Xu, Z., Liu, X., Chen, L., Dai, J., Karrow, N.A., Sun, L., 2021. Occurrence of aflatoxin B1, deoxynivalenol and zearalenone in feeds in China during 2018–2020. J. Anim. Sci. Biotechnol. 12, 74. https://doi.org/10.1186/s40104-021-00603-0.
Zhou, J.-Y., Zhang, S.-W., Lin, H.-L., Gao, C.-Q., Yan, H.-C., Wang, X.-Q., 2019. Hydrolyzed wheat gluten alleviates deoxynivalenol-induced intestinal injury by promoting intestinal stem cell proliferation and differentiation via upregulation of Wnt/β-catenin signaling in mice. Food Chem. Toxicol. Int. J. Publ. Br. Ind. Biol. Res. Assoc. 131, 110579 https://doi.org/10.1016/j.fct.2019.110579.